Neutron pickup strength in ^{87}Sr from the $(\vec{p},d)$ reaction

M. C. Radhakrishna,* N. G. Puttaswamy,* H. Nann, D. W. Miller, P. P. Singh, W. W. Jacobs, W. P. Jones, and E. J. Stephenson

Department of Physics and Indiana University Cyclotron Facility, Bloomington, Indiana 47405

(Received 30 May 1989)

Differential cross section and analyzing power angular distributions have been obtained for the ^{87}Sr$(\vec{p},d)^{86}$Sr reaction in two measurements using different magnetic spectrometers at incident proton energies of 94.2 and 91.8 MeV. Typical energy resolutions of 70 and 40 keV, respectively, were achieved. Optical-model parameters were obtained by fitting the elastic scattering data measured to laboratory angles of 90° for protons at 94.2 MeV and to 120° for deuterons at 88.0 MeV. Standard exact finite range distorted-wave Born approximation calculations using these optical-model parameters failed to describe the experimental data, while the adiabatic approximation improved the description to some extent. Orbital and total angular momenta, l and j, of the picked-up neutron were extracted from the angular distributions of the differential cross section and analyzing power for all the residual states observed. The rms radius of the $1g_{9/2}$ neutron orbital, obtained from magnetic electron scattering, was used in the extraction of strength for this orbital, while rms radii from Hartree-Fock calculations were used for the $2p_{1/2}$, $2p_{3/2}$, $1f_{5/2}$, and $1f_{7/2}$ orbitals. The observed $1g_{9/2}$ strength, spread over 20 states up to 5.4-MeV excitation, indicates a depletion of about 43% compared to simple shell-model expectations. Similarly, the observed $1f_{5/2}$ strength, spread over 17 states, indicates a depletion of about 32%. The weighted summed spectroscopic strength for the $1g_{9/2}$ orbital, deduced from the present study, is lower than that obtained from magnetic electron scattering.

I. INTRODUCTION

There has been a great deal of interest recently in the question as to whether the orbitals near the Fermi surface of closed-shell nuclei show depletion in their occupation numbers. Both theoretical predictions[1–3] and experimental results[4–10] have in fact shown significant reduction in the occupation numbers for nuclei in the lead region due to a combination of short-range, tensor, and long-range correlations. Historically, one-nucleon transfer reactions are known to yield useful information about the centroid positions and filling rates of single-particle states near the nuclear Fermi surface. It has usually been assumed that the distorted-wave Born approximation (DWBA) correctly describes the reaction mechanism. However, due to many uncertainties involved in the DWBA ingredients, the extraction of reliable spectroscopic information has been questionable. It has been common practice to renormalize the extracted relative spectroscopic factors so that their total sums *agree* with spectroscopic sum rules. Often the bound-state radius parameter (to which the extracted spectroscopic factors are very sensitive) is chosen quite arbitrarily, and this is the cause for the major portion of the uncertainty in the predicted DWBA cross section. Of course contributions to the total uncertainty can also arise from inadequate optical potentials used to generate the distorted waves. In this paper we report a systematic study of the ^{87}Sr$(\vec{p},d)^{86}$Sr reaction, where care is taken to minimize the uncertainties that enter into the DWBA calculations, hence maximizing the reliability of the extracted spectroscopic strengths.

First of all, this study was chosen because the bound-state wave function of the $1g_{9/2}$ valence neutron is accurately known from magnetic electron scattering[11–14] on ^{87}Sr. In particular, Platchkov *et al.*[12] determined the root-mean-square (rms) radii of valence orbitals for several nuclei by using elastic magnetic electron scattering in order to isolate experimentally the highest possible magnetic multipole in the high-momentum-transfer region. The rms radius measured for the $1g_{9/2}$ bound neutron in ^{87}Sr in its ground state[12] is 4.823 fm (4.756 fm) with (without) the inclusion of meson exchange current (MEC) corrections. This radius, measured to an accuracy of 1%, provides a very important input to the DWBA calculations for determining the spectroscopic strength for pickup from the $1g_{9/2}$ orbital.

In order to reduce the uncertainties associated with the optical potentials, elastic scattering measurements were made for both entrance and exit channels. In a similar study of the ^{206}Pd$(\vec{d},^3$He$)^{205}$Tl reaction,[10] we have obtained a good DWBA description of the experimental data, and have extracted spectroscopic factors to an accuracy of about 15–20 %. However, unlike the $(d,^3$He) reaction, the experimental data on (p,d) reactions are not described adequately by the standard DWBA calculations, mainly because of the breakup in the deuteron channel. If breakup effects are taken into account by using the adiabatic approximation, then data are in general better described.

The ground state of the ^{87}Sr nucleus can be thought of as a simple $1g_{9/2}$ neutron hole in ^{88}Sr. When a $1g_{9/2}$ neutron is picked up in the ^{87}Sr$(\vec{p},d)^{86}$Sr reaction, ^{86}Sr is left in a $(g_{9/2})^{-2}$ two-hole configuration, leading to a multi-

plet with spins 0^+, 2^+, 4^+, 6^+, and 8^+, all of which are excited by $l=4$ transitions. Of course, negative-parity states in ^{86}Sr are also populated through $l=1$ and/or $l=3$ transfer. We here use both the standard well depth (WD) and the more recent surface-peak (SP) methods[10] to generate the target form factor required in the DWBA calculations. The SP method takes into account the residual interaction which splits states of a given configuration. The rms radius measured from magnetic electron scattering is used for the $1g_{9/2}$ orbital, while rms radii from Hartree-Fock calculations (normalized to that of the $1g_{9/2}$ orbital) are used for other orbitals.[15]

Neutron pickup from ^{87}Sr with the (p,d) reaction has been reported earlier by Kitching *et al.*,[16] whose data were subsequently reanalyzed by Moalem and Friedman.[17] In a recent study of the (d,t) reaction, Li *et al.*[18] have identified the levels in ^{86}Sr up to 3.823-MeV excitation energy; $1g_{9/2}$ strength was observed only up to 3.481 MeV. In the present paper our results will be compared with these earlier transfer reaction results and also with the results of elastic magnetic electron scattering.

The experimental procedures used in the present investigation are described in Sec. II, while the analyses carried out to obtain the best fit optical-model parameters are outlined in Sec. III. Exact finite-range distorted-wave analyses are presented in Sec. IV, and a discussion of the results of the present study is given in Sec. V.

II. EXPERIMENTAL PROCEDURE

The ^{87}Sr$(\vec{p},d)^{86}$Sr reaction was studied using 94.2-MeV and 91.8-MeV polarized proton beams at the Indiana University Cyclotron Facility. Angular distributions of differential cross section $\sigma(\theta)$ and analyzing power $A_y(\theta)$ were measured. Data at 94.2-MeV bombarding energy were taken with a quadrupole-dipole-dipole-multipole (QDDM) magnetic spectrometer (hereafter referred to as QDDM data), while data at 91.8 MeV were obtained with the newly commissioned K600 magnetic spectrometer (hereafter referred to as K600 data). The outgoing deuterons (for QDDM data) were detected between laboratory angles ($\theta_{\rm lab}$) of 6° and 38° in 2° or 3° steps; for the K600 data they were detected between 6° and 23° at similar intervals. In order to obtain optical-model parameters required for the DWBA calculations, elastic-scattering measurements of both $\sigma(\theta)$ and $A_y(\theta)$ were made with the QDDM spectrometer for protons on ^{87}Sr at 94.2 MeV, and for deuterons on ^{86}Sr at 88.0 MeV. The elastically scattered protons from ^{87}Sr were detected between $\theta_{\rm lab}$ of 9° and 90° in 1° or 2° steps. The energy of the deuterons for elastic scattering from ^{86}Sr was chosen to match the center-of-mass of the ground-state transition energy for the time-reversed reaction, after taking the Q value of the ^{87}Sr$(\vec{p},d)^{86}$Sr reaction into account. Deuterons scattered elastically from ^{86}Sr were observed between $\theta_{\rm lab}$ of 7° and 33° in 1° steps, between 33° and 80° in 3° or 4° steps, and between 90° and 120° in 10° steps.

The proton beam polarizations were about $+0.80$ and -0.79 for the two spin orientations, and were measured periodically during the course of the experiment with a ^{4}He polarimeter placed between the injector and the main cyclotron by observing elastic scattering at $\theta_{\rm lab}=112°$. The vector polarization of the deuterons was measured by inserting a ^{3}He polarimeter into the same beam line and observing protons from the ^{3}He$(d,p)^4$He reaction at $\theta_{\rm lab}=12°$. Typical vector polarizations of the deuteron beam were $+0.58$ and -0.60. Other details of these procedures have been described previously.[10]

The $(\vec{p},d)$ reaction and elastic scattering products were momentum analyzed in the QDDM (K600) magnetic spectrometer and detected in the focal plane with a position-sensitive helical proportional counter (vertical drift chambers), followed by two plastic scintillators for particle identification. Overall energy resolutions of about 70 (40) keV were achieved with the QDDM (K600) magnetic spectrometer.

The target materials used in the experiment with the QDDM spectrometer, supplied by Oak Ridge National Laboratory (ORNL), were 84.88% isotopically enriched ^{87}Sr (which also contained 13.84% of ^{88}Sr as contaminant) and 96.89% isotopically enriched ^{86}Sr. The ^{87}Sr targets were fabricated by reducing $SrCO_3$ with aluminum in vacuum, then further reduced, distilled, and rolled under mineral oil to thicknesses of 5.0 and 10 mg/cm^2. The ^{86}Sr targets of thickness 4.2 and 11.7 mg/cm^2 were made by rolling. In order to cross normalize the thicknesses of these targets, elastic scattering measurements were made at selected angles on a 97.62% isotopically enriched, 4.1-mg/cm^2 thick ^{90}Zr target, made by rolling. All measured differential cross sections were normalized to the value obtained with the ^{90}Zr target, whose thickness had been previously measured accurately. Measurements of cross sections with the various targets were repeated at selected angles to check reproducibility.

As mentioned above, the target used in taking the ^{87}Sr$(\vec{p},d)$ data with the QDDM spectrometer had 13.84% of ^{88}Sr as contaminant. The Q-value difference between the ^{87}Sr$(\vec{p},d)^{86}$Sr and the ^{88}Sr$(\vec{p},d)^{87}$Sr reactions is 2.685 MeV. Thus, the ground state of the latter reaction overlaps with the 2.674-MeV state of the former reaction. Other excited states of the ^{88}Sr$(\vec{p},d)$ reaction overlap with ten corresponding states of the ^{87}Sr$(\vec{p},d)$ reaction spectrum, as depicted in Fig. 1. Unfortunately, during data acquisition with the QDDM spectrometer, we did not have a ^{88}Sr target in order to subtract the contribution from this contaminant. Therefore, we recently carried out the (p,d) reaction on both the isotopes ^{87}Sr and ^{88}Sr using the K600 magnetic spectrometer. As this experimental run was a very short one, a proton beam of energy 91.8 MeV (delivered to a previous user) was used without attempting to change the energy to 94.2 MeV. However, we assume that the results obtained at 94.2 and 91.8 MeV will not be significantly different for the purpose of the present comparison. The target materials supplied by ORNL, and used in this short K600 run, were isotopically enriched ^{87}Sr (which contained 87.76% ^{87}Sr and 10.85% ^{88}Sr), and 99.84% isotopically enriched ^{88}Sr. Both the ^{87}Sr and ^{88}Sr targets, each of thickness 5.0 mg/cm^2, were made by rolling. Elastic-scattering measurements were again made on the ^{87}Sr, ^{88}Sr, and ^{90}Zr targets to normalize the cross sections to the value ob-

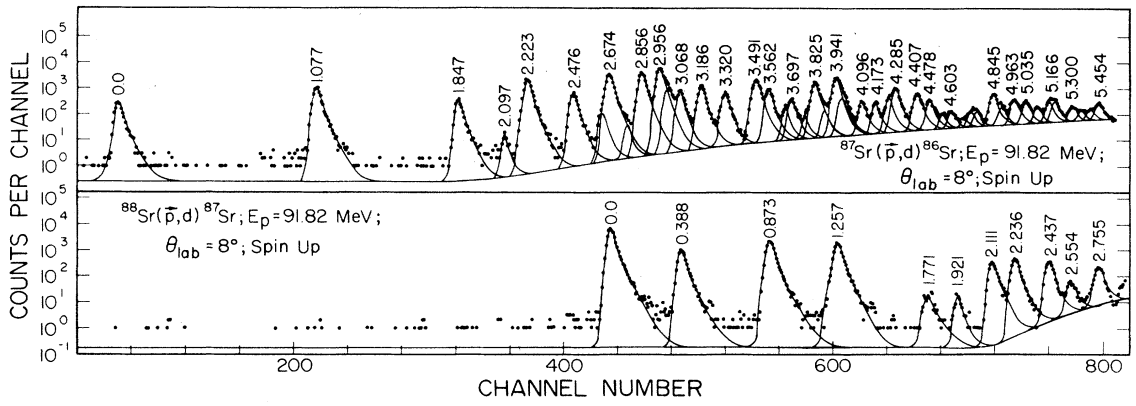

FIG. 1. Semilog plot of the deuteron energy spectrum, using proton spin-up orientation, for the ^{87}Sr$(\vec{p},d)^{86}$Sr reaction at a bombarding energy of 91.82 MeV taken with the K600 spectrometer at beam left $\theta_{lab}=8°$. The positions of peaks corresponding to states in ^{86}Sr are indicated by their excitation energies in MeV, and the solid curve indicates the fit to the spectrum obtained with the fitting procedure described in the text.

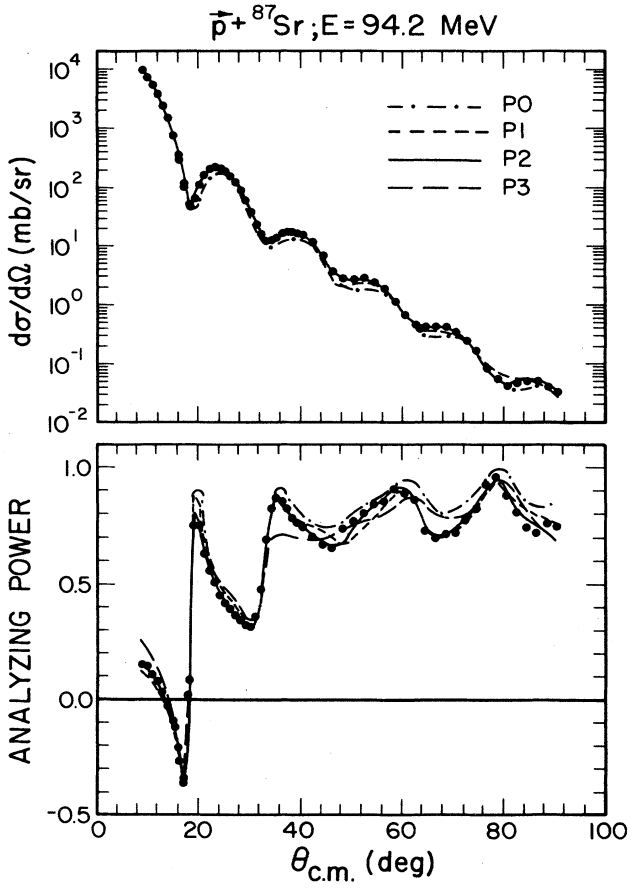

FIG. 2. Differential cross-section and analyzing-power angular distributions for elastic scattering of 94.2-MeV protons from ^{87}Sr. The curves represent different optical-model parametrizations as described in the text.

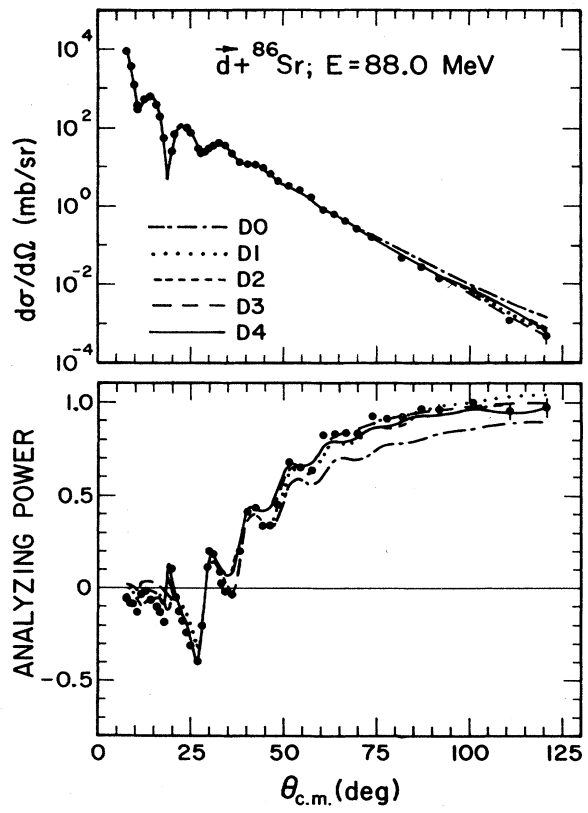

FIG. 3. Differential cross-section and analyzing-power angular distributions for elastic scattering of 88.0-MeV deuterons from ^{86}Sr. The curves represent different optical-model parametrizations as described in the text.

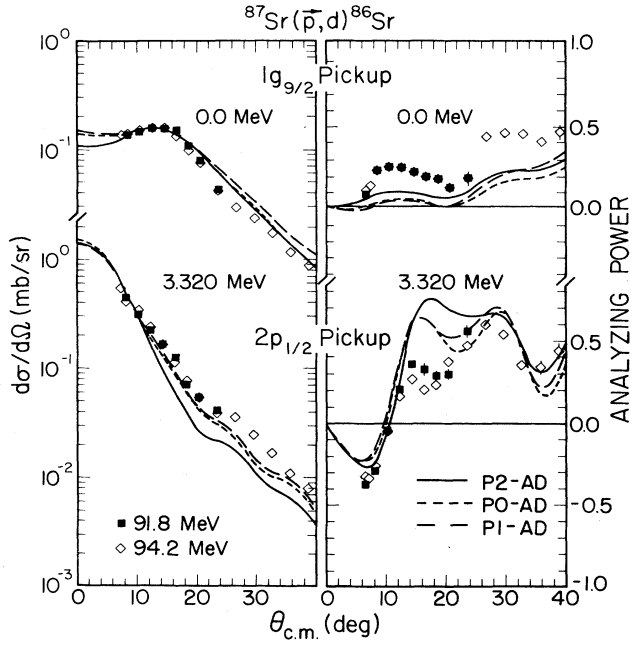

FIG. 4. Angular distributions of differential cross section and analyzing power for the ground state and 3.32-MeV transitions in the ^{87}Sr$(\vec{p},d)^{86}$Sr reaction at 94.2-MeV bombarding energy. The curves are the results of standard ADWA calculations using different sets of proton optical-model parameters described in the text.

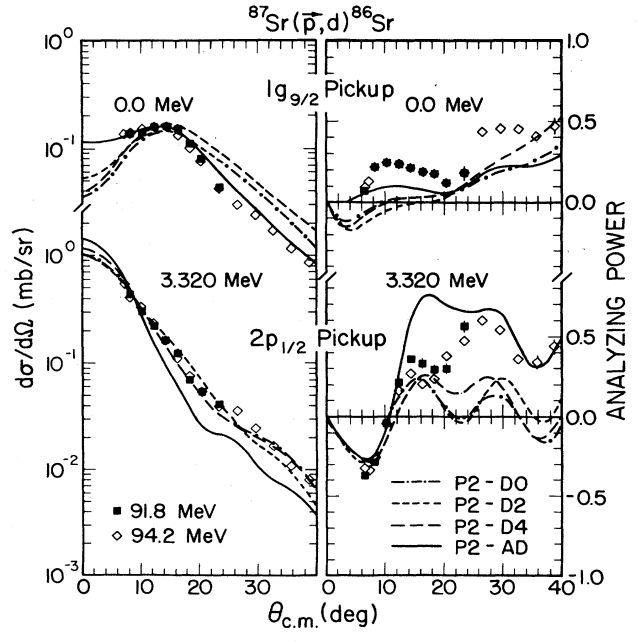

FIG. 5. Angular distributions of differential cross section and analyzing power for the ground state and 3.32-MeV transitions in the ^{87}Sr$(\vec{p},d)^{86}$Sr reaction at 94.2-MeV bombarding energy. The curves are the results of standard DWBA calculations using different sets of deuteron optical-model parameters described in the text.

tained with the comparison 4.1-mg/cm^2 ^{90}Zr target.

The particle spectra were analyzed with the computer code ALLFIT.[20] Typical deuteron spectra for the ^{87}Sr$(\vec{p},d)^{86}$Sr and ^{88}Sr$(\vec{p},d)^{87}$Sr reactions taken with the K600 spectrometer at $\theta_{lab}=8°$ are shown in Fig. 1. Peak areas were obtained by fitting the spectra using a hyper-Gaussian peak shape whose parameters had been obtained by fitting the shape of the peak corresponding to

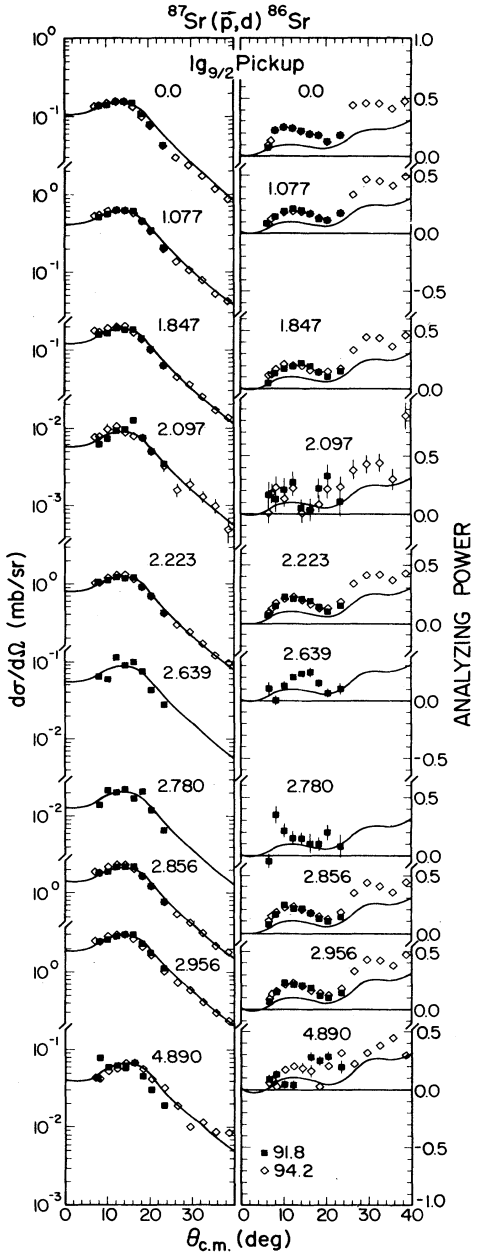

FIG. 6. Angular distributions of differential cross section and analyzing power for $1g_{9/2}$ ($l=4$) transitions in the ^{87}Sr$(\vec{p},d)^{86}$Sr reaction at 94.2-MeV bombarding energy. The curves represent exact finite-range ADWA calculations using the parameter sets *P*2-AD, and the SP method for the radial form factor.

the fourth excited state of ^{86}Sr as a standard. Spectra from the reaction ^{88}Sr$(\vec{p},d)^{87}$Sr were also fitted using the same hyper-Gaussian peak shape, but with parameters obtained by fitting the shape of the ground state of ^{87}Sr. Both spin-up and spin-down spectra were analyzed simultaneously with the same widths and common peak shapes, thus helping to reduce systematic errors. The cross sections and analyzing powers were calculated from individual peak areas of the spin-up and spin-down spectra. Error bars shown in the angular distributions (Figs. 2–9) reflect only counting statistics. The nominal $\theta_{lab}=6°$ cross sections were rejected because of the fact that the internal Faraday cup was partially obscuring about $\frac{1}{3}$ of the entrance opening of both the QDDM and K600 spectrometers at this most forward angle; the analyzing powers at this angle could be retained but the measured

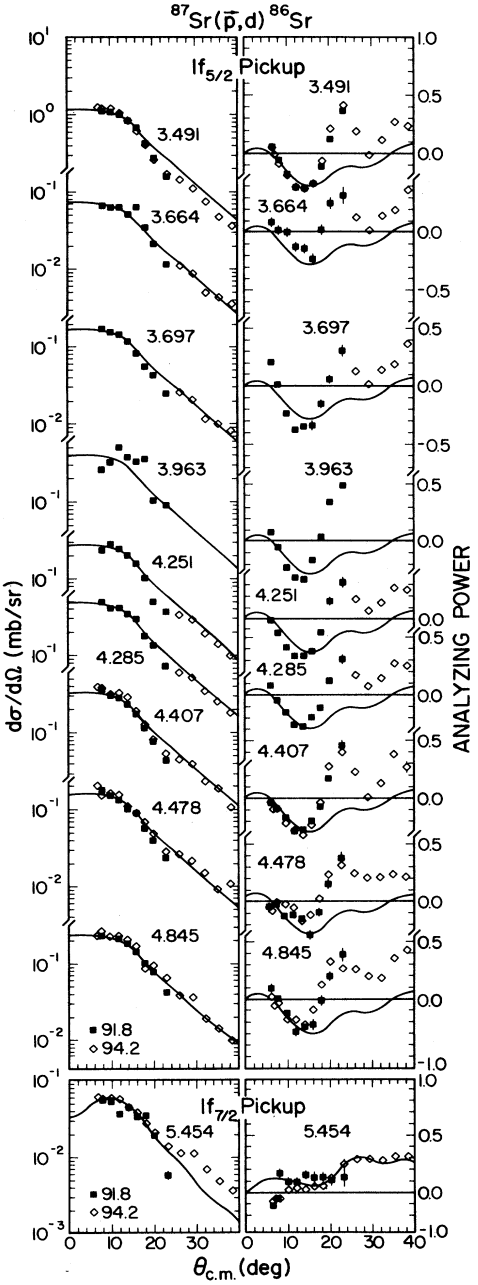

FIG. 7. Angular distributions of differential cross section and analyzing power for $1f_{5/2}$ and $1f_{7/2}$ ($l=3$) transitions. For further details see caption to Fig. 6.

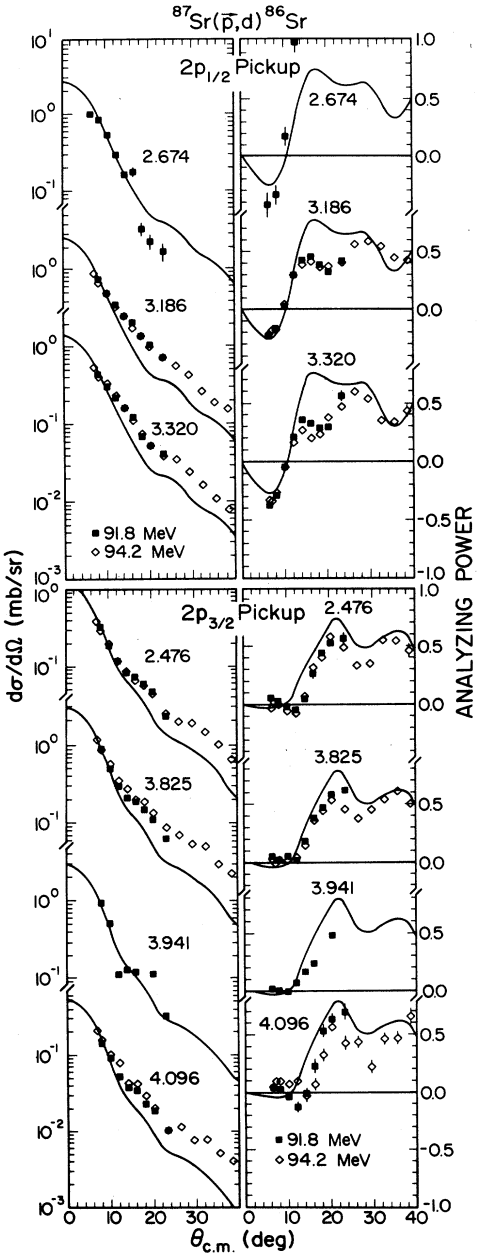

FIG. 8. Angular distributions of differential cross section and analyzing power for $2p_{1/2}$ and $2p_{3/2}$ ($l=1$) transitions. For further details see caption to Fig. 6.

TABLE I. Energy levels of ^{86}Sr.

Present results		Nuclear data sheets[a]		^{87}Sr$(d,t)^{86}$Sr[b]		^{88}Sr$(\vec{p},t)^{86}$Sr[c]		
E_x (keV)	nlj	E_x (keV)	J^π	l_{tr}	J^π assumed	E_x (keV)	l_{tr}	J^π
0	$1g_{9/2}$	0	0^+	4	0^+	0	0	0^+
1077±5	$1g_{9/2}$	1077[d]	2^+	2,4	2^+	1077	2	2^+
1847±5	$1g_{9/2}$	1854	2^+	2,4	2^+	1855	2	2^+
2097±5	$1g_{9/2}$	2102	0^+	4	0^+	2102	0	0^+
		2203	0^+	4	0^+	2202	0	0^+
2223±5	$1g_{9/2}$	2230	4^+	2,4	4^+	2230	4	4^+
2476±5	$2p_{3/2}$	2482	3^-	1	3^-	2480	3	3^-
		2497	(0,1,2)					
2639±5	$1g_{9/2}$	2642	(2^+)	2,4	$(2)^+$	2641(3)	2	2^+
2674±5	$2p_{1/2}$	2673	5^-	1	5^-	2668	5	5^-
2780±5	$1g_{9/2}$	2788	(2^+)	2,4	$(2)^+$	2785	2	2^+
2856±5	$1g_{9/2}$	2857	(6^+)	2,4	$(6)^+$	2856	6	6^+
		2878	$(4)^+$	(0),2				
2956±5	$1g_{9/2}$	2955[d]	(8^+)	4	$(8)^+$	2957	8	8^+
2995±5	$1g_{9/2},2p_{3/2}$	2997	3^-	1	3^-	2997	3	3^-
		3045	(0,1,2)					
3068±10	$1g_{9/2},2p_{1/2}$	3055	$(5)^-$	1	$(5)^-$	3057	5	5^-
		3101	(0^+)	4	$(0)^+$	3106	(2)	(2^+)
3186±10	$2p_{1/2}$	3185	(3^-)	1	$(4)^-$			
						3192	(2)	(2^+)
		3291	$(3,4^-)$	1				
3320±10	$2p_{1/2}$	3318	(5^-)	1	$(5)^-$			
						3328	4	4^+
		3362	(4^+)	2,4	$(4)^+$	3360	0	0^+
		3392	$(1-4)^+$			3377	2	2^+
		3430	(2^+)			3443	2	2^+
		3481	(6^+)			3499		
3491±10	$1f_{5/2}$			3,4	$(2^-\text{-}7^-),(4^+)$	3499	7	7^-
		3500	$(3,4,5)^-$	1				
3664±10	$1f_{5/2}$	3645	3^-			3660	4	4^+
3697±10	$1f_{5/2}$	3687	$(3,4^+)$					
						3708	2	2^+
		3766	$(3^-,4^-)$					
3772±10	$1g_{9/2},2p_{1/2}$	3775				3790	(3)	(3^-)
3825±10	$2p_{3/2}$	3823[d,e]		(1)				
		3831	$(3^-,4^-,5^-)$			3835	5	5^-
3882±10	$1f_{5/2}$	3872						
						3900	(3)	(3^-)
		3926	$(4,5)^+$					
3941±10	$2p_{3/2}$	3943						
						3948	4	4^+
3963±10	$1f_{5/2}$	3969				3967	5	(5^-)
4096±10	$2p_{3/2}$							
		4146				4148	2	2^+
4173±10	$(1g_{9/2},2p_{3/2})$							
		4206				4207		
4251±10	$1f_{5/2}$							
4285±10	$1f_{5/2}$					4287	(2)	(2^+)
		4339				4328	4	4^+
4407±10	$1f_{5/2},2p_{3/2}$	4410						
						4409	(2)	(2^+)
4478±15	$1f_{5/2},2p_{3/2}$							
						4486	0	0
4526±15	$1f_{5/2}$							
						4558	4	4^+
		4590						
4603±15	$1f_{5/2}$							
		4645						
4665±15	$(1g_{9/2})$	4657						

TABLE I. (*Continued*).

Present results		Nuclear data sheets[a]		^{87}Sr$(d,t)^{86}$Sr[b]		^{88}Sr$(\vec{p},t)^{86}$Sr[c]		
E_x (keV)	nlj	E_x (keV)	J^π	l_{tr}	J^π assumed	E_x (keV)	l_{tr}	J^π
4716±15	$(1g_{9/2})$	4718						
4738±15	$(1f_{5/2})$							
4845±20	$1f_{5/2}$							
4890±15	$1g_{9/2}$							
4963±20	$1g_{9/2},2p_{3/2}$	4954						
5035±20	$1g_{9/2},2p_{3/2}$							
5102±15	$(1f_{5/2})$							
5166±20	$(1f_{5/2})$							
5191±20	$(1g_{9/2},1f_{7/2})$							
5300±20	$(1f_{5/2})$							
5357±20	$(1g_{9/2},2p_{1/2})$							
5403±20	$(1f_{5/2})$							
5454±20	$(1f_{7/2})$							

[a] Reference 21.
[b] Reference 18.
[c] Reference 22.
[d] Energy level values used for the present calibration.
[e] Energy level established by Ref. 22.

angle was corrected to 6.4°.

The energy calibrations of the spectra were carried out by fitting quadratic polynomials to the deuteron momenta as a function of channel number. Relativistic kinematics were used. Due to the improvement in the energy resolution with the K600 magnetic spectrometer, the number of reliably extractable peaks in the spectra was 46 compared to the 32 peaks in the spectra taken with QDDM. Thus, we quote in Table I the excitation energies for ^{86}Sr levels obtained from this experiment with the K600, along with the values determined from previous studies.[18,21,22]

III. OPTICAL-MODEL ANALYSES

Differential cross section $\sigma(\theta)$ and analyzing power $A_y(\theta)$ angular distributions of 94.2-MeV elastically scattered protons from ^{87}Sr and 88.0-MeV elastically scattered deuterons from ^{86}Sr are shown in Figs. 2 and 3, respectively. An optical-model prediction using the global optical-model parameter set of Schwandt *et al.*[23] for protons on ^{87}Sr is displayed as the dot-dashed line labeled *P*0. Although oscillatory structures in the angular distributions for both $\sigma(\theta)$ and $A_y(\theta)$ are similar to those observed in our data, the prediction nonetheless fails to reproduce the $\sigma(\theta)$ data in magnitude between 20° and 90°, and overestimates $A_y(\theta)$ beyond 40°.

For deuterons the global optical-model parameters of Daehnick *et al.*[24] for ^{86}Sr predict larger cross sections at the larger angles and underestimate the analyzing power between 50° and 120°. These predictions are shown as the dot-dashed curve *D*0 in Fig. 3. Given these results from the global analysis, we have therefore systematically analyzed the elastic scattering data from the present study in the conventional framework of the optical model in order to search for parameters which would more adequately describe the data specific to this investigation.

A. Optical potential

The data analyses were performed with a 13-parameter optical-model potential including complex central and spin-orbit parts using the automatic search code GOMFIL developed by Leeb.[25] The complex potential was of the form

$$V(r)=V_C(r)-V_R(1+e^{x/\alpha})^{-\alpha}-iW_s(1+e^{y/\beta})^{-\beta}+i4W_D(d/dy)(1+e^{y/\beta})^{-\beta}$$
$$-2\left[\frac{\hbar}{m_\pi c}\right]^2[V_{so}f_{so}(r)+iW_{so}f_{ws}(r)](\vec{l}\cdot\vec{S}) , \quad (1)$$

with

$$x=(r-r_0A^{1/3})/a_0 \quad \text{and} \quad y=(r-r_wA^{1/3})/a_w .$$

The exponents α,β of the nuclear potential form factors can be chosen different from unity in order to modify the real or imaginary central potential, viz., a Woods-Saxon (WS) form for $\alpha=1$, or a squared Woods-Saxon (WS^2) form for $\alpha=2$, without changing the asymptotic falloff which remains as $\sim e^{-r/a}$. The real and imaginary spin-orbit form factors were of the conventional Thomas type:

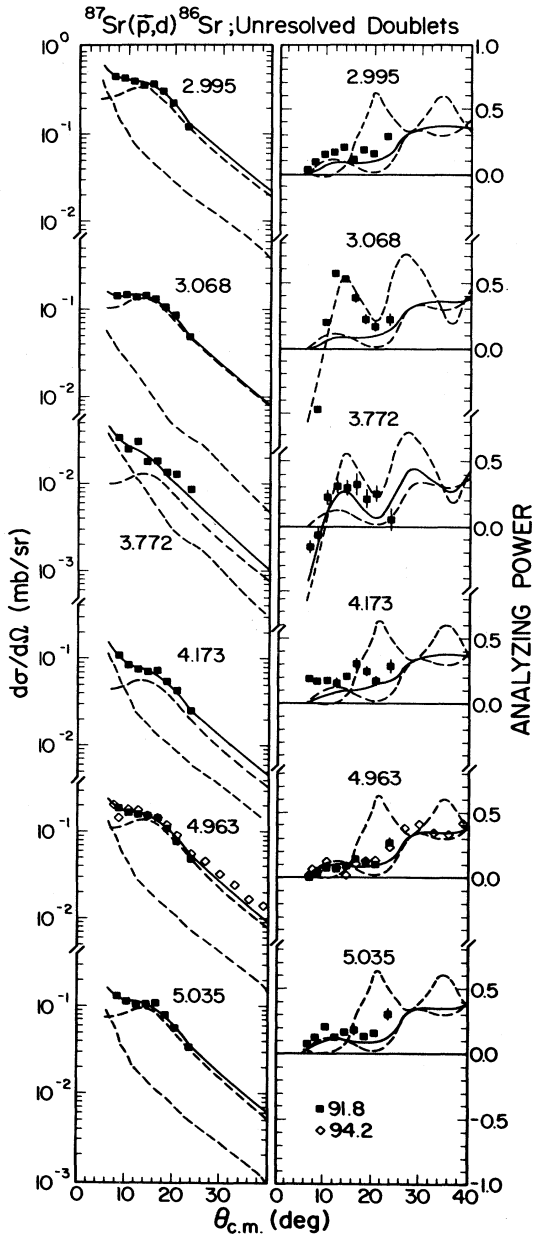

FIG. 9. Angular distributions of differential cross section and analyzing power for typical unresolved states in the ^{87}Sr$(\vec{p},d)^{86}$Sr reaction at 94.2-MeV bombarding energy. Contributing l- and j-values (see Table I) are shown as dashed lines. The composite angular distributions are shown as solid lines.

$$f_{so}(r)=(1/r)(d/dr)(1+e^{s})^{-1},$$
$$\text{with } s=(r-r_{so}A^{1/3})/a_{so} \quad (2)$$

and

$$f_{ws}(r)=(1/r)(d/dr)(1+e^{t})^{-1},$$
$$\text{with } t=(r-r_{ws}A^{1/3})/a_{ws}\ . \quad (3)$$

In the fitting procedure, the influence of the cross-section data on the final results would have been much greater than that of the analyzing-power data, because of the smaller statistical uncertainties in $\sigma(\theta)$ as compared to those in $A_y(\theta)$. Therefore, in the present analyses, the uncertainty for the differential cross-section data was taken as 2% for all angles for which the actual error was less than 2%. On the other hand, a constant error of 1.5% was assigned to analyzing-power data at those angles for which the actual error was less than 1.5%. By using these different weightings for $\sigma(\theta)$ and $A_y(\theta)$, the $A_y(\theta)$ description was improved considerably with almost no visible change in the fit to $\sigma(\theta)$; the latter result is expected from the low sensitivity of the differential cross section to the spin-orbit-potential parameters.

B. Proton elastic scattering from ^{87}Sr

Starting parameters to fit the proton elastic scattering data on ^{87}Sr were taken from various earlier proton elastic scattering studies. Using the parameters of Schwandt *et al.*[23] (labeled $P0$ and having no surface imaginary part), the resulting best-fit parameters yielded the curve labeled $P1$ in Fig. 2. Extrapolated parameters from Becchetti and Greenlees[26] gave a best-fit set which is shown as curve $P3$ in Fig. 2. This particular set does not have an imaginary part of the spin-orbit potential. None of the above starting parameter sets gave an acceptable best fit to the experimental data. Finally, we followed the procedure used by den Herder *et al.*[27] in their study of the ^{90}Zr $(e,e'p)$ reaction, where two outgoing proton energies, $T_p=70$ and 100 MeV, were used. Here the geometry parameters for volume and surface imaginary potentials are different, thus increasing the number of parameters by three. This method does give a satisfactory fit to both cross-section and analyzing-power data. The resulting fit from these parameters is shown by the solid curve $P2$ in Fig. 2. The different sets of optical-model parameters are listed in Table II.

TABLE II. Optical-model parameters for proton elastic scattering from ^{87}Sr at 94.2 MeV.

Set	V_R (MeV)	r_0 (fm)	a_0 (fm)	W_S (MeV)	W_D (MeV)	r_w (fm)	a_w (fm)	V_{so} (MeV)	r_{so} (fm)	a_{so} (fm)	W_{so} (MeV)	r_{ws} (fm)	a_{ws} (fm)	r_c (fm)	J/A (MeV/fm^3)	σ_r (mb)	χ^2/point
$P0$	29.66	1.219	0.7042	7.00		1.424	0.5555	4.19	1.055	0.655	−0.955	1.037	0.62	1.25	263	1011	68
$P1$	30.33	1.239	0.6736	7.599		1.466	0.4974	4.93	1.079	0.656	−1.143	1.048	0.422	1.25	278	1111	11
$P2$	26.89	1.280	0.6490	7.25[a]	2.80	1.331	0.5271	3.99	1.116	0.620	−1.343	1.065	0.442	1.25	267	1174	4
$P3$	25.96	1.283	0.7712	6.24	4.30	1.072	0.7146	2.98	1.302	0.754				1.30	271	957	32

[a] Here W_S has different geometry viz., $r_s=1.183$ fm, and $a_s=1.089$ fm.

TABLE III. Optical-model parameters for deuteron elastic scattering from ^{86}Sr at 88.0 MeV.

Set	Type	V_R (MeV)	r_0 (fm)	a_0 (fm)	W_S (MeV)	W_D (MeV)	r_w (fm)	a_w (fm)	V_{so} (MeV)	r_{so} (fm)	a_{so} (fm)	W_{so} (MeV)	r_{ws} (fm)	a_{ws} (fm)	r_c (fm)	J/A (MeV/fm^3)	σ_r (mb)	χ^2/point
$D0$	WS(global)	73.20	1.170	0.8586	7.81	6.68	1.325	0.8243	2.39	1.070	0.660				1.30	313	1931	61
$D1$	WS	71.77	1.189	0.8228	7.95	7.69	1.298	0.8087	2.43	1.046	0.761				1.30	314	1905	30
$D2$	WS+ISO	69.94	1.208	0.7996	8.45	7.51	1.297	0.8029	2.07	1.015	0.671	−0.645	0.819	0.377	1.30	315	1893	18
$D3$	WS^2	82.70	1.344	0.6207	9.36	5.43	1.320	0.8788	2.62	1.008	0.767				1.30	301	1956	20
$D4$	WS^2+ISO	80.19	1.353	0.611	10.33	4.26	1.328	0.9228	2.50	0.937	0.733	−0.555	0.743	0.309	1.30	298	1981	14

C. Deuteron elastic scattering from ^{86}Sr

Starting parameters for deuteron scattering on ^{86}Sr (labeled $D0$) were taken from the global set of Daehnick *et al.*[24] At first, the radial shape of the real potential was taken to have the standard Woods-Saxon (WS) form, and searches were made to obtain the best fit without restriction on any of the parameters. However, the use of the WS form of the potential produced analyzing powers at small angles that did not reproduce the structure observed in the data; the resulting curve is shown as curve $D1$ in Fig. 3. As a next step, an imaginary spin-orbit term [see Eq. (3)] was added to the potential (WS+ISO), and an extensive 13-parameter search was made. This form of the potential gave a reasonably good fit (curve $D2$) to the analyzing-power data.

In order to investigate the influence of the radial shape of the potential form on the fit, a change was made from a WS form to a squared Woods-Saxon (WS^2) form. This alteration did not produce any significant improvement in the quality of the fit compared to that of the WS form of the potential (see curve $D3$ in Fig. 3). However, when an imaginary spin-orbit term was added to the potential (WS^2+ISO), there was a significant improvement in the quality of fit for the analyzing-power data at large angles (see the curve $D4$ in Fig. 3).

Similar deuteron elastic scattering studies on ^{206}Pb at an energy of 79.4 MeV have been reported,[10] where different potential shapes were also tried. Both (WS+ISO) and (WS^2+ISO) potential forms gave a better description of the analyzing-power data at large angles, as was the case here for $d+^{86}$Sr. However, the effect of the imaginary spin-orbit term in the potential is more pronounced for ^{206}Pb.

The different sets of deuteron optical-model parameters obtained from the present study are listed in Table III.

IV. DISTORTED-WAVE ANALYSES

Exact-finite-range DWBA calculations were performed for all the observed transitions employing the computer code DWUCK5.[28] Two prescriptions were used to carry out these calculations. The first one was standard DWBA, where the distorted waves in both entrance and exit channels were generated from the optical-model parameters that describe the elastic scattering data as discussed in the previous section. The second was the adiabatic prescription (ADWA) to be discussed later, where the optical potential for deuterons is replaced by the adiabatic potential. In both cases the nonlocality corrections $\beta=0.85$ fm^2 for protons and $\beta=0.54$ fm^2 for deuterons were applied. However, no nonlocality correction was used for the bound-state wave function. The light-particle form factor $V_{np}\phi_d$ was obtained from the Reid soft core potential[29] which includes both the S and D states of the deuteron. The target form factor was generated by employing well-depth and surface-peak methods as described in detail later. The spectroscopic strength G was extracted using the relation

$$\left[\frac{d\sigma}{d\Omega}\right]_{\text{exp}} = Gg\left[\frac{d\sigma}{d\Omega}\right]_{\text{DW5}}, \tag{4}$$

where $(d\sigma/d\Omega)_{\text{exp}}$ is the experimentally measured differential cross section, $(d\sigma/d\Omega)_{\text{DW5}}$ is the differential cross section predicted by the DWUCK5 code, and g is the light-particle spectroscopic strength which is here equal to 1.0. We note, that $G=C^2S$, where C is an isospin Clebsch-Gordan coefficient, and S is the spectroscopic factor.

A. The standard DWBA calculation

The standard method employed in performing distorted-wave calculations involves the use of optical-model potentials that describe the elastic scattering data of both entrance and exit channels. For the calculations described in this paper, best fit optical-model parameters, listed in Tables II and III, were used to generate the distorted waves. Sample DWBA and ADWA predictions are shown in Figs. 4 and 5 for the ground-state ($l=4$) and 3.320-MeV state ($l=1$), transitions in the ^{87}Sr$(\vec{p},d)^{86}$Sr reaction. In order to examine the sensitivity to the choice of entrance- and exit-channel optical-model potential sets, calculations were performed for various combinations of potential sets. The curves in Fig. 4 were generated with a fixed deuteron potential (AD) and various proton potential sets, $P0$, $P1$, and $P2$ as listed in Table II. These different sets of proton potentials gave essentially the same cross section and analyzing power distribution shapes, except for the set $P2$, which gave the best description of the experimental $l=4$ transition. Next, calculations (shown in Fig. 5) were carried out with different sets of deuteron optical-model parameters $D0$, $D2$, and $D4$ listed in Table III in combination with the proton optical potential set $P2$. In general, the predicted distributions are poor for the $1g_{9/2}$ transfer data, even though the angular momentum is well matched for $l=4$ at this energy. However, the description of the cross section data for the $l=1$ transition (which is mismatched in angular momentum) is good for all the deuteron potentials. In summary, the standard DWBA approach does not describe the data very well, even though the various ingredients to the calculations have been specified as well as they possibly can be.

B. The adiabatic approximations (ADWA)

It is widely believed that the inadequacy in describing deuteron stripping and pickup reactions arises mainly because of the weakly-bound structure of the deuteron. This suggests the relevance of three-body effects in the reaction mechanism. In the conventional DWBA approach, one describes the deuterons by the elastic-scattering wave function generated from optical-model potentials fitted to describe the elastic scattering data. In the adiabatic prescription (ADWA),[30] which includes breakup effects in the analyses of stripping and pickup data, the elastic deuteron wave function is replaced by a three-body wave function which treats the low-energy relative s-wave n-p breakup effects in an effective range manner. The key feature of the adiabatic theory is the derivation of an effective potential—the adiabatic potential—which generates the appropriate three-body wave function from an effective two-body Schrödinger equation. In practice, the adiabatic potential is derived from neutron and proton optical potentials obtained from fits to nucleon elastic scattering data at half the deuteron energy. Inclusion of breakup effects give a geometry to this potential which is significantly different from that of conventional deuteron phenomenological optical potentials. This feature is largely responsible for eliminating the need for an arbitrary suppression of the interior contributions to stripping integrals when the adiabatic wave function is used. Johnson and Tandy[31] have further improved the adiabatic theory, by using a slightly different adiabatic potential which is essentially the folding of the nucleon-core potentials over the shape of the short-ranged V_{np}. The resulting geometry in the center-of-mass coordinate system has additional important differences from that of phenomenological elastic deuteron optical potentials.

The adiabatic potential (AD) for deuterons was generated from Eq. (34) of Ref. 31. The global nucleon-nucleus potential parameters of Becchetti and Greenlees[26] were folded with the soft-core interaction and corresponding deuteron wave function of Reid.[29] This potential was then fitted to a Woods-Saxon form to get numerical potential parameters to be used in the code DWUCK5. The resultant parameters are listed as set AD in Table IV.

ADWA calculations were performed with all the best-fit proton parameter sets listed in Table II, along with the AD set for deuterons, for the ground-state transition. The description of the data was found to be far better with the combination $P2$ and AD than with any other pair of parameter sets, as is evident from Figs. 4 and 5. Thus the parameter sets $P2$ for protons and AD for deuterons were used in all the remaining calculations described herein. The results are quoted in Tables VI through X.

C. The target form factor

The target form factor, which contains the nuclear structure information, is usually generated by the "well-

TABLE IV. Adiabatic potentials of deuterons for ^{86}Sr at 88.95 MeV. The entry in this table is for ground-state transition. For excited states well depths given by $V=V-(E-85.93)\times0.32$, $W_S=W_S+(E-85.93)\times0.22$, and $W_D=W_D-(E-85.93)\times0.25$ were used. E is the outgoing deuteron energy in MeV.

Set	Type	V_R (MeV)	r_0 (fm)	a_0 (fm)	W_S (MeV)	W_D (MeV)	r_w (fm)	a_w (fm)	V_{so} (MeV)	r_{so} (fm)	a_{so} (fm)	r_c (fm)
AD	WS(adiabatic)	85.301	1.1622	0.7977	15.327	1.774	1.300	0.6476	3.1	1.010	0.750	1.30

TABLE V. Bound state parameters.[a]

Set	Method	V_0 (MeV)	V_{sur} (MeV)	r_0 (fm)	a_0 (fm)	V_{sc}[b] (MeV)	r_{so} (fm)	a_{so} (fm)
$B1$	WD	varied[c]	0.0	fixed[d]	0.650	7.00	1.10	0.65
$B2$	SP	fixed[e]	varied[f]	fixed[d]	0.650	7.00	1.10	0.65

[a] No nonlocality is used for the bound state.
[b] $4V_{so}$ is used in DWUCK5.
[c] Adjusted to match the separation energy of each state.
[d] The bound-state radius parameter r_0 was fixed at 1.262, 1.187, 1.210, 1.205, and 1.223 fm respectively, for $1g_{9/2}$, $1f_{5/2}$, $1f_{7/2}$, $2p_{1/2}$, and $2p_{3/2}$ orbitals.
[e] The well depths V_0 were fixed at −48.73, −49.22, −48.90, −48.06, and −47.71 MeV respectively, for the $1g_{9/2}$, $1f_{5/2}$, $1f_{7/2}$, $2p_{1/2}$, and $2p_{3/2}$ orbitals; the resulting rms radii were respectively 4.792, 4.323, 4.409, 4.437, and 4.367 fm for the corresponding centroids.
[f] The surface-peaked potential was assumed to be of the derivative WS form and the depth of the surface peak was adjusted to match the separation energy of the state.

depth" (WD) method: the depth of a Woods-Saxon potential is adjusted until the separation energy of the picked-up particle from the specified orbital is matched. In these calculations we chose the measured rms radius for the $1g_{9/2}$ orbital as measured in magnetic electron scattering.[12] Actually a value of 4.79 fm was used for this parameter after correction was made for the centroid energy of the $(1g_{9/2})^{-2}$ multiplet, and conversion to the intrinsic frame. For other orbitals we used rms radii from HF calculations[15] scaled down by about 0.6% in order to match the calculated and measured rms radius for the $1g_{9/2}$ orbital. The bound-state radius parameter (r_0) and the potential depth (V_0) were varied until the separation energy of the energy centroid was matched, fixing the rms radius constant. The resulting bound-state parameters are listed as set $B1$ in Table V.

Another approximation for calculating the form factor has been suggested by Austern[32] and Rae,[33] and has been used by Winfield *et al.*[34] in a study of the (^{9}Be, ^{10}B) reaction. This method, called the surface-peak (SP) method, was successfully used in our analysis of the ^{206}Pb$(\vec{d},{}^3$He$)^{205}$Tl reaction.[10] Here, a fixed mean-field potential plus an additional surface-peaked potential is used to describe the motion of the transferred nucleon. The

TABLE VI. Spectroscopic strength G for $1g_{9/2}$ neutron pickup in ^{86}Sr.

E_x (MeV)	J^π	$(\vec{p},d)$ 94.2 MeV[a] SP method	$(\vec{p},d)$ 94.2 MeV[a] WD method	(d,t) reaction[b]	(d,t) reaction reanalysis[c]	(p,d) reaction reanalysis[d]
0.0	0^+	0.13±0.02	0.09±0.02	0.13	0.13	0.18±0.02
1.077	2^+	0.46±0.08	0.38±0.07	0.58	0.51	0.70±0.09
1.847	2^+	0.13±0.02	0.13±0.02	0.21	0.15	0.25±0.03
2.097	0^+	0.006±0.001	0.010±0.002	0.013	0.009	
2.223	4^+	0.85±0.15	0.84±0.15	1.28	0.92	0.14±0.02
2.639	2^+	0.06±0.01	0.06±0.01	0.107	0.068	
2.780	2^+	0.013±0.03	0.013±0.003	0.03	0.016	
2.856	6^+	1.45±0.26	1.48±0.27	2.40	1.56	2.27±0.30
2.956	8^+	1.96±0.35	2.03±0.36	3.46	2.32	2.94±0.25
2.995		0.22±0.05	0.23±0.05			
3.068		0.082±0.02	0.086±0.02			
3.772		0.010±0.003	0.011±0.003			
4.173		0.04±0.01	0.04±0.01			
4.665		0.009±0.002	0.012±0.003			
4.716		0.024±0.007	0.024±0.007			
4.890		0.04±0.01	0.05±0.01			
4.963		0.081±0.02	0.102±0.02			
5.035		0.057±0.016	0.072±0.020			
5.191		0.021±0.006	0.026±0.007			
5.357		0.012±0.003	0.015±0.004			
$\Sigma G(1g_{9/2})=$		5.68±1.04	5.72±1.06	8.64	5.88	6.48±0.7

[a] Present experiment.
[b] Reference 18.
[c] Present reanalysis with the SP method using the bound-state parameters of Table V.
[d] Reference 17.

TABLE VII. Spectroscopic strength G for $1f_{5/2}$ neutron pickup in ^{86}Sr.

E_x (MeV)	$(\vec{p},d)$ 94.2 MeV[a] SP method	WD method	(d,t) reaction[b]
3.491	1.354±0.34	1.220±0.31	0.66
3.664	0.083±0.34	0.077±0.025	
3.697	0.188±0.05	0.175±0.04	
3.882	0.087±0.02	0.085±0.02	
3.963	0.432±0.21	0.421±0.21	
4.251	0.289±0.09	0.298±0.10	
4.285	0.507±0.13	0.523±0.13	
4.407	0.342±0.10	0.362±0.10	
4.478	0.165±0.05	0.174±0.06	
4.526	0.039±0.02	0.042±0.02	
4.603	0.054±0.02	0.058±0.02	
4.738	0.042±0.02	0.046±0.02	
4.845	0.233±0.06	0.265±0.07	
5.102	0.063±0.02	0.076±0.02	
5.166	0.087±0.05	0.105±0.06	
5.300	0.063±0.02	0.078±0.02	
5.403	0.047±0.02	0.059±0.02	
$\Sigma G(1f_{5/2})=$	4.075±1.25	4.064±1.24	

[a] Present experiment.
[b] Reference 18.

TABLE VIII. Spectroscopic strength G for $1f_{7/2}$ neutron pickup in ^{86}Sr.

E_x (MeV)	$(\vec{p},d)$ 94.2 MeV[a] SP method	WD method
5.191	0.16±0.08	0.16±0.08
5.454	0.08±0.03	0.08±0.03
$\Sigma G(1f_{7/2})=$	0.24±0.11	0.24±0.11

[a] Present experiment.
[b] Reference 18.

TABLE IX. Spectroscopic strength G for $2p_{1/2}$ neutron pickup in ^{86}Sr. The uncertainty of the extracted spectroscopic factors is ≥30%.

E_x (MeV)	$(\vec{p},d)$ 94.2 MeV[a] SP method	WD method	(d,t) reaction[b]
2.674	1.05	1.01	0.95
3.068	0.05	0.05	0.06
3.186	0.86	0.87	0.68
3.320	0.51	0.52	0.34
3.772	0.02	0.02	
5.357	0.02	0.03	
$\Sigma G(2p_{1/2})=$	2.51	2.50	2.03

[a] Present experiment.
[b] Reference 18.

TABLE X. Spectroscopic strength G for $2p_{3/2}$ neutron pickup in ^{86}Sr. The uncertainty of the extracted spectroscopic factors is ≥30%.

E_x (MeV)	$(\vec{p},d)$ 94.2 MeV[a] SP method	WD method	(d,t) reaction[b]
2.476	0.61	0.52	0.24
2.995	0.31	0.28	
3.825	1.17	1.19	0.83
3.941	1.07	1.10	
4.096	0.19	0.20	
4.173	0.07	0.08	
4.963	0.09	0.12	
5.035	0.06	0.08	
$\Sigma G(2p_{3/2})=$	3.57	3.57	1.07

[a] Present experiment
[b] Reference 18.

parameters that describe the mean-field potential are chosen to yield the right predetermined energy centroids of individual orbitals with specific rms radii. Furthermore, following the suggestion of Millener and Hodgson,[35] the depths of the potentials for each orbit in the SP method were calculated to match the energy centroids previously determined from the spectroscopic strengths deduced with the WD method. The depth of the additional surface-peaked potential is varied to match the separation energy of the transferred particle, thus ensuring the correct tail shape of the form factor. The surface-peaked potential can be interpreted as simulating the effects of the residual interaction at the nuclear surface. Of course, for closed-shell nuclei, the WD and SP methods yield the same results, since the SP potential term must then be zero. The potential parameters used in the present study for the calculation of the form factor by the SP method are listed as set $B2$ in Table V.

V. RESULTS AND DISCUSSION

Transitions corresponding to 45 excited states were observed in the present experiment. Several new states were seen. The angular momentum transfers we have assigned from the present analysis to states up to 3 MeV agree with known spin-parity assignments. Both WD and SP methods were used in the present study to deduce the spectroscopic strengths for all of the 46 observed peaks. The $\sigma(\theta)$ calculated using the ADWA prescription was fitted to the data using a least-squares method; however, greater weighting was given to the cross sections measured at the five most forward angles.

The ADWA predictions for the angular distributions of the differential cross section and analyzing power using the SP method are shown in Figs. 6 to 9 for the ^{87}Sr$(\vec{p},d)^{86}$Sr reaction; these include neutron pickup from the $1g_{9/2}$, $1f_{5/2}$, $1f_{7/2}$, $2p_{1/2}$, and $2p_{3/2}$ orbitals. Different j transfers involved in the present study were established by taking as experimental templates the j-dependent angular patterns from an earlier neutron pickup study[36] of the ^{86}Sr$(\vec{p},d)^{85}$Sr reaction. This was necessary, because the shape predictions from the distorted

wave calculations were found to be generally unreliable for such identifications.

The spectroscopic strengths extracted from the present study are listed in Tables VI–X. Also given are the results from the (d,t) reaction.[18] Even though the SP and WD methods give roughly the same summed spectroscopic strengths, the actual values for individual states may differ by as much as 25% (e.g., in the case of the 5.403-MeV state). Such effects are due mainly to the fact that the rms radius in the WD method decreases with excitation energy (relative to the centroid energy), whereas in the SP method it increases with excitation energy; of course both have the same rms radii at the respective energy centroids.

The component of $l=2$ transition strength observed for the 1.077, 1.847, 2.223, 2.639, 2.780, and 2.856-MeV states by the previous ^{87}Sr(d,t) study[18] at 18 MeV is not seen in the present investigation. This may perhaps be due to the angular momentum mismatch for $l=2$ at 94 MeV, which suppresses the $l=2$ strength relative to the $l=4$ strength. The 2.995-MeV state is found to include $1g_{9/2}$ pickup strength which is not seen by the previous studies,[16–18] indicating the presence of a positive-parity state in addition to the 3^- state. States at 3.055 and 3.101 MeV seen in the previous work with much higher resolution could not be resolved in the present experiment with 40-keV resolution. Hence both $2p_{1/2}$ and $1g_{9/2}$ strengths contribute to the transition at 3.068 MeV. A small amount of $l=4$ strength noticed by Li *et al.*[18] for the 3.362-MeV state is not seen in the present study. The 3.491-MeV state has a clear signature of $1f_{5/2}$ pickup, suggesting only a negative-parity assignment.

Since the energy resolution in this particular study was about 40 keV, quite a few states lying close to one another could not be resolved. As a result, angular distributions of some of the observed peaks contained two transitions. For such multiplets, known experimental templates of both cross section and analyzing power were used to disentangle the l and j transfers involved. The procedure involved a least-square fitting of the observed cross-section angular distribution with the known experimental templates. These "disentangled" experimental data are then compared with the respective ADWA curves in order to extract the spectroscopic factors. The analyzing power of each such doublet was calculated by weighting the analyzing powers of the individual contributions by the corresponding cross sections. Figure 9 shows typical angular distributions of $\sigma(\theta)$ and $A_y(\theta)$ for some of the observed doublets. The solid line in both $\sigma(\theta)$ and $A_y(\theta)$ shows the empirical prediction obtained from the known templates; the dashed lines show the individual components involved.

A. States with $1g_{9/2}$ transfer

The ADWA predictions for transitions involving $1g_{9/2}$ transfer are shown in Fig. 6. It is clear from the figure that even though the differential cross sections are described reasonably well, the analyzing-power data are poorly described. The $A_y(\theta)$ data are reproduced quantitatively in both shape and phase but are severely underestimated throughout the angular range. The observed $1g_{9/2}$ strength is spread over 20 states. Table VI lists the spectroscopic strength for the $1g_{9/2}$ orbital compared with that obtained from the (d,t) reaction studies of Li *et al.*[18] who observed $1g_{9/2}$ strength only up to 3.481 MeV of excitation energy. The spectroscopic factors seen in the present study are much lower compared to the corresponding spectroscopic factors from the (d,t) study. These discrepancies were thought to be mainly due to differences in the form factor description and also to the choice of the bound-state parameters in the DWBA analysis of the (d,t) reaction. Therefore, the (d,t) data were reanalyzed using our bound-state parameters and employing the SP method. The results obtained from this reanalysis are now in reasonable agreement with our $(\vec{p},d)$ results. Also compared in Table VI are the spectroscopic factors obtained by Moalem and Friedman[17] from a reanalysis of the (p,d) data of Kitching *et al.*[16] In their reanalysis they considered only $l=4$ transitions, employed a variety of optical potentials in both entrance and exit channels, and performed DWBA calculations applying full finite-range and nonlocality corrections using an rms radius of 4.66 fm for the $1g_{9/2}$ orbital. This rms radius is lower than our value and hence their spectroscopic factors are consistently higher for all the individual states except for the 2.223-MeV state, where their spectroscopic factor is about six times smaller than ours. Yet, their summed spectroscopic strength of 6.48 is larger than our results, even though they analyzed only the strong $l=4$ transitions.

B. States with $1f_{5/2}$ and $1f_{7/2}$ transfer

The ADWA for transitions involving $1f_{5/2}$ and $1f_{7/2}$ transfers together with the data are shown in Fig. 7. The most striking j-dependent feature is the negative slope of $A_y(\theta)$ from 10°–13° for the $1f_{5/2}$ transfer as compared to the positive or near-zero values for the $1f_{7/2}$ transfer. Clearly the oscillatory pattern of the $A_y(\theta)$ data is not accounted for except at smaller angles, although the positions of maxima and minima are reproduced. The spectroscopic strengths extracted from the present study for $1f_{5/2}$ and $1f_{7/2}$ orbitals are listed and compared with results of the (d,t) study[18] in Tables VII and VIII, respectively. In the (d,t) study, although states up to 3.823 MeV in excitation were observed, $l=3$ strength is seen only at 3.491 MeV and not at 3.664 or 3.697 MeV, where some of the $l=3$ strength is seen in the present study. Furthermore, an overall $l=3$ strength of 0.66 extracted from the (d,t) study is almost a factor of two less than the strength observed in the present work. In the (d,t) study, at 3.491 MeV both $l=3$ and 4 transitions are identified based only upon the shape of the cross section angular distribution. On the other hand, in the present investigation no $l=4$ component is seen for this state, based on the shape of both cross section and analyzing-power angular distributions.

While we see that the $1f_{5/2}$ strength spreads over 17 states, $1f_{7/2}$ strength is seen only for two transitions. This indicates that most of the $1f_{7/2}$ strength lies at higher excitation energies outside the range of observa-

tion in the present work. In this regard it may be noted that in the (p,d) study on ^{90}Zr by Taketani *et al.*,[19] $1f_{7/2}$ strength is seen up to 12.2 MeV in excitation.

C. States with $2p_{1/2}$ and $2p_{3/2}$ transfer

Figure 8 shows the results obtained for the $2p_{1/2}$ and $2p_{3/2}$ transfers. Though the fits to the $\sigma(\theta)$ data are not good, the description of $A_y(\theta)$ is generally satisfactory even for these momentum mismatched transitions. As the $l=1$ transfer experimental cross sections are most forward peaked, there is larger uncertainty in the $l=1$ extracted spectroscopic factors than those for the $l=3$ and 4 transitions, due to the normalization at these most forward angles. This introduces an uncertainty which is difficult to assess. We estimate that the error for the spectroscopic factors of the $2p_{1/2}$ and $2p_{3/2}$ transitions is at least 30%. However, even considering these large assigned uncertainties, the summed strength for the $2p_{1/2}$ orbital exceeds the simple shell-model sum rule, indicating that the rms radius used from HF calculations is too small. For the $2p_{3/2}$ orbital, the extracted strength is close to the sum rule value, which is perhaps fortuitous. A 2% increase in the bound-state radius parameter would give spectroscopic strengths for these orbitals consistent with the depletion observed for the $1g_{9/2}$ and $1f_{5/2}$ orbitals.

The errors quoted in Tables VI through VIII include the following uncertainties combined in quadrature: (i) 5% due to target thickness; (ii) 5–40 % due to the peak fitting procedure; (iii) 5% due to proton optical potentials; (iv) 10% due to deuteron adiabatic potentials; (v) 5% due to the deuteron form factor; (vi) 10–15 % due to bound-state parameters; and (vii) 5–40 % due to the least-squares fit to the transfer-reaction data.

The errors in items (ii) and (vii) varied depending on the statistics of the data involved, while errors in items (iii) and (iv) were due to the difference in the ADWA predictions when different sets of adiabatic deuteron potentials and different proton optical-model parameters were used. Finally, the 10–15 % error in item (vi) due to the target bound-state parameters results mainly from a change in the bound-state radius parameter (r_0) by 1% (which is about the uncertainty in r_0).

In order to interpret the spectroscopic factors for the valence $1g_{9/2}$ orbital in ^{87}Sr, we apply two (spin-dependent) sum rules. The first one is the partial sum rule which, for a given orbital, connects the single-nucleon stripping and pickup spectroscopic factors of an odd target nucleus. The expression is[37]

$$S_{J_f}^{-}=\frac{2J_f+1}{2J_0+1}-(2J_f+1)(-1)^{2J_0+1}\sum_{J_f'}\begin{Bmatrix} J_f' & j & J_0 \\ J_f & j & J_0 \end{Bmatrix} S_{J_f'}^{+} \ . \tag{5}$$

Here $S_{J_f'}^{+}$ and $S_{J_f}^{-}$ are the partial sums of spectroscopic factors for stripping and pickup reactions to final states J_f' and J_f, respectively, and J_0 is the spin of the odd target nucleus. Reanalyzing the ^{87}Sr$(d,p)^{88}$Sr data of Li and Daehnick[38] using the SP method to generate the transfer form factor, and employing the rms radius from magnetic electron scattering,[12] we get a spectroscopic strength $S^{+}=0.78$ for the $1g_{9/2}$ orbital. Using Eq. (5) one obtains partial sums of spectroscopic factors of 0.18, 0.89, 1.60, 2.31, and 3.03 for the final states with spin and parity 0^+, 2^+, 4^+, 6^+, and 8^+, respectively. The partial sums obtained in the present study for the final states with known J^π (see Table VI) are 0.14, 0.66, 0.85, 1.45, and 1.96. They are about 22–46 % lower than those calculated with the partial sum rule. Some of the missing strength resides in the other $1g_{9/2}$ transitions observed. Since the final-state J^π values of these other $1g_{9/2}$ transitions are not known, this comparison is incomplete.

The second sum rule relates the (magnetic) spectroscopic strength ρ_9 obtained from elastic magnetic electron scattering to a sum over spectroscopic factors. For pickup this relationship is[39]

$$\rho_\lambda^{(\alpha)}=(2J_0+1)\times\sum_{J_f T_f}(-1)^{J_0+J_f+j_\alpha+\lambda}\begin{Bmatrix} J_0 & J_0 & \lambda \\ j_\alpha & j_\alpha & J_f \end{Bmatrix} S_{J_f,T_f}^{-}(\alpha) \ . \tag{6}$$

Here λ is the multipolarity of the electromagnetic transition, α the single-particle orbital of interest, and J_0, J_f are the spins of the initial and final states. Using again only the spectroscopic factors for the $1g_{9/2}$ transitions to final states with known J^π values ($E_x \le 2.96$ MeV) we obtain $\rho_9=0.62$. This value is smaller than the result of $\rho_9=0.76\pm0.05$ obtained from magnetic electron scattering.[12] Here again the comparison is incomplete. However, our value is considerably larger than the value of 0.49 which Dieperink and Sick[39] have deduced in reanalyzing the data of Ref. 17.

Recently Kunz[40] suggested some improvements to the form of nonlocality used in the optical potentials and also an energy dependence of the adiabatic deuteron potential used in the adiabatic prescription. The former is a nonlocality correction based upon the Darwin term[41] and is calculated from the spin orbit potential. The latter is an improvement related to the adiabatic deuteron potential which suggests that, instead of using half the deuteron energy for calculating the nucleon potentials, an external energy dependence has to be added.[42] Both of these modifications were tried in this study, but neither of them was found to yield improvement in the agreement of the theory with the data.

Roy and Mukherjee[43,44] have recently estimated the deuteron breakup contribution by solving an integral equation. They have developed a simple prescription for estimating the effect of the breakup channel using optical-model parameters fitted to elastic deuteron scattering. It would be interesting to attempt fits to our data using such an approach, and in particular to look at the description of the $A_y(\theta)$ data.

VI. CONCLUSIONS

A systematic study of the ^{87}Sr$(\vec{p},d)^{86}$Sr reaction has been made in order to extract the spectroscopic factors

with reasonable accuracy. Optical-model parameters used in the exact finite-range DWBA calculations for both entrance and exit channels were obtained from direct fitting of measured elastic-scattering data, at the appropriate bombarding energies. Unfortunately, these conventional, exact finite-range DWBA calculations failed to reproduce the transfer data, so that adiabatic approximation, exact finite-range ADWA calculations were then performed. A realistic deuteron form factor generated by employing the Reid soft-core wave function was used. However, the angular distributions of cross section and analyzing power were still not well reproduced by the ADWA calculations, even for the $l=4$ transitions which have a good angular-momentum match at $E_p=94.2$ MeV. The bound-state rms radius of the $1g_{9/2}$ orbital was fixed at the value extracted from magnetic electron scattering, and the rms radii of other orbitals were taken from the predictions of Hartree-Fock calculations (scaled down by about 0.6% to match the $1g_{9/2}$ rms radius), in order to avoid large uncertainties in the extracted spectroscopic factors. The alternate "well-depth" and "surface-peak" methods employed to generate the bound-state form factor gave similar total spectroscopic strengths, although extracted strengths for individual states differed by as much as 25%. The neutron pickup strengths determined in the present study with the SP method are 5.68, 4.08, 0.23, 2.53, and 3.57 for the $1g_{9/2}$, $1f_{5/2}$, $1f_{7/2}$, $2p_{1/2}$, and $2p_{3/2}$ transfers respectively. When compared to the simple shell-model sum rule values of 9, 6, 8, 2, and 4, for the same respective transfers, we observe a quenching of about 43% for $1g_{9/2}$ transfer, and 32% for $1f_{5/2}$ transfer. The almost full strength obtained for the $2p_{1/2}$ and $2p_{3/2}$ orbitals is probably fortuitous (e.g., the rms radii obtained from HF calculations for the $2p_{1/2}$ and $2p_{3/2}$ orbitals may be too small, resulting in larger spectroscopic factors for these two cases). Most of the strength for the $1f_{7/2}$ orbital lies at $E_x>5.5$ MeV and hence was not observed in the present experiment. The spectroscopic quantity $\rho_9=0.62\pm0.12$ calculated from the present study is in fair agreement with the magnetic electron scattering result of 0.76 ± 0.05. This comparison is incomplete since many $1g_{9/2}$ transitions are left out because they lead to final states whose spins are not known.

Although the adiabatic prescription is a better approximation than conventional DWBA for describing the experimental (p,d) pickup data, it is still far from satisfactory. At this point we do not fully understand the shortcomings of either the DWBA or ADWA in explaining the data. The results seem to require much greater damping of the contributions of the low partial waves to the transfer integral than is provided by nonlocality and finite-range.

ACKNOWLEDGMENTS

We gratefully acknowledge numerous discussions with P. D. Kunz, and express our appreciation to him for making available to us the latest version of the code DWUCK5. We also wish to thank J. Tostevin for making available to us the deuteron adiabatic potentials used in this study. Thanks are also due to B. A. Brown for making available to us the Hartree-Fock calculations. The assistance of P. Schwandt during data acquisition and analysis of the data is gratefully acknowledged. We also thank G. P. A. Berg and R. Sawafta for helping us with the data acquisition with the K600 magnetic spectrometer. This work was supported in part by National Science Foundation Grant No. PHY 84-12177.

*Permanent address: Department of Physics, Bangalore University, Bangalore 560 001, India.

[1]D. Gogny, in *Nuclear Physics with Electromagnetic Interactions,* Vol. 108 of *Lecture Notes in Physics,* edited by H. Arenhovel and D. Drechsel (Springer-Verlag, Berlin, 1979), p. 88.

[2]V. R. Pandharipande, C. N. Papanicolas, and J. Wambach, Phys. Rev. Lett. **53**, 1133 (1984).

[3]M. Jaminon, C. Mahaux, and H. Ngo, Nucl. Phys. **A440**, 228 (1985).

[4]J. M. Cavedon, B. Frois, D. Goutte, M. Huet, Ph. Leconte, C. N. Papanicolas, X. H. Phan, S. K. Platchkov, and S. Williamson, Phys. Rev. Lett. **49**, 978 (1982).

[5]B. Frois, J. M. Cavedon, D. Goutte, M. Huet, Ph. Leconte, C. N. Papanicolas, X. H. Phan, S. K. Platchkov, and S. E. Williamson, Nucl. Phys. **A396**, 409c (1983).

[6]E. N. M. Quint, J. F. J. van den Brand, J. W. A. den Herder, E. Jans, P. H. M. Keizer, L. Lapikás, G. van der Steenhoven, P. K. A. de Witt Huberts, S. Klein, P. Grabmayr, G. J. Wagner, H. Nann, B. Frois, and D. Goutte, Phys. Rev. Lett. **57**, 186 (1986).

[7]E. N. M. Quint, B. M. Barnett, A. M. van den Berg, J. F. J. van den Brand, H. Clement, R. Ent, B. Frois, D. Goutte, P. Grabmayr, J. W. A. den Herder, E. Jans, G. J. Kramer, J. B. J. M. Lanen, L. Lapikas, H. Nann, G. van der Steenhoven, G. J. Wagner, and P. K. A. de Witt Huberts, Phys. Rev. Lett. **58**, 1088 (1987).

[8]P. Grabmayr, S. Klein, H. Clement, K. Reiner, W. Reuter, G. J. Wagner, and G. Seegert, Phys. Lett. **164B**, 15 (1985).

[9]H. Clement, P. Grabmayr, H. Röhm, and G. J. Wagner, Phys. Lett. B **183**, 127 (1987).

[10]M. C. Radhakrishna, N. G. Puttaswamy, H. Nann, J. D. Brown, W. W. Jacobs, W. P. Jones, D. W. Miller, P. P. Singh, and E. J. Stephenson, Phys. Rev. C **37**, 66 (1988).

[11]T. W. Donnelly and I. Sick, Rev. Mod. Phys. **56**, 461 (1984).

[12]S. K. Platchkov, J. B. Bellicard, J. M. Cavedon, B. Frois, D. Goutte, M. Huet, P. Leconte, Phan Xuan Hô, and P. K. A. de Witt Huberts, Phys. Rev. C **25**, 2318 (1982).

[13]P. K. A. de Witt Huberts, L. Lapikás, and I. Sick, Nucl. Phys. **A396**, 71c (1983).

[14]I. Sick, J. B. Bellicard, J. M. Cavedon, B. Frois, M. Huet, P. Leconte, A. Nakada, Phan Xuan Hô, S. Platchkov, P. K. A. de Witt Huberts, and L. Lapikás, Phys. Rev. Lett. **38**, 1259 (1977).

[15]B. A. Brown (private communication).

[16]J. E. Kitching, W. Darcey, W. G. Darcey, W. G. Davies, W. McLatchie, and J. M. Morton, Phys. Lett. **32B**, 343 (1970).

[17]A. Moalem and E. Friedman, Phys. Rev. Lett. **40**, 1064 (1978).

[18]P. C. Li, W. W. Daehnick, and R. D. Rosa, Nucl. Phys. **A442**, 253 (1985).
[19]H. Taketani, M. Adachi, M. Ogawa, and K. Ashibe, Nucl. Phys. **A204**, 385 (1973).
[20]J. J. Kelly, University of Maryland, Program Manual, ALLFIT, 1983 (unpublished).
[21]J. W. Tepel, Nucl. Data Sheets **25**, 553 (1978).
[22]A. Saha, Ph.D. thesis, Northwestern University, 1976 (unpublished).
[23]P. Schwandt, H. O. Meyer, W. W. Jacobs, A. D. Bacher, S. E. Vigdor, M. D. Kaitchuck, and T. R. Donoghue, Phys. Rev. C **26**, 55 (1982).
[24]W. W. Daehnick, J. D. Childs, and Z. Vrcelj, Phys. Rev. C **21**, 1127 (1980).
[25]H. Leeb, General Optical Model Fitting Code, Atomic Institute of Austrian Universities, Vienna, 1984 (unpublished).
[26]F. D. Becchetti, Jr. and G. W. Greenlees, Phys. Rev. **182**, 1190 (1969).
[27]J. W. A. Den Herder, E. Jans, P. H. M. Keizer, L. Lapikás, E. N. M. Quint, P. K. A. De Witt Huberts, H. P. Block, and G. van der Steenhoven, Phys. Lett. B **184**, 11 (1987).
[28]P. D. Kunz, Computer code DWUCK5, and extended as FRUCK2 by J. R. Comfort, Indiana University Cyclotron Facility Internal Report No. 85-1, 1985 (unpublished).
[29]R. V. Reid, Jr., Ann. Phys. (N.Y.) **50**, 411 (1968).
[30]R. C. Johnson and P. J. R. Soper, Phys. Rev. C **1**, 976 (1970); J. D. Harvey and R. C. Johnson, *ibid.* **3**, 636 (1971).
[31]R. C. Johnson and P. C. Tandy, Nucl. Phys. **A235**, 56 (1974).
[32]N. Austern, Nucl. Phys. **A292**, 190 (1977).
[33]W. D. M. Rae, Ph.D. thesis, Oxford University, 1976 (unpublished).
[34]J. S. Winfield, N. A. Jelley, W. D. M. Rae, and C. L. Woods, Nucl. Phys. **A437**, 65 (1985).
[35]D. J. Millener and P. E. Hodgson, Nucl. Phys. **A209**, 59 (1973).
[36]H. Nann, D. W. Miller, W. W. Jacobs, D. W. Devins, W. P. Jones, and Li Qing-li, Phys. Rev. C **27**, 1073 (1983).
[37]C. F. Clement and S. M. Perez, Nucl. Phys. **A284**, 469 (1977).
[38]P. C. Li and W. W. Daehnick, Nucl. Phys. **A462**, 26 (1987).
[39]A. E. L. Dieperink and I. Sick, Phys. Lett. **109B**, 1 (1982).
[40]P. D. Kunz (private communication).
[41]B. C. Clark, R. L. Mercer, and P. Schwandt, Phys. Lett. **122B**, 211 (1983).
[42]P. D. Kunz, in *Notas de Fisica,* Proceedings of the Tenth Oaxtepec Symposium on Nuclear Physics, edited by A. Menchaca-Rocha (Instituto de Fisica, UNAM, Mexico City, 1987).
[43]T. K. Roy and S. Mukherjee, J. Phys. G **13**, 957 (1987).
[44]T. K. Roy and S. Mukherjee, J. Phys. G **13**, 1239 (1987).